Journal of Alloys and Compounds 498 (2010) 162–167

Contents lists available at ScienceDirect

Journal of Alloys and Compounds

journal homepage: www.elsevier.com/locate/jallcom

Composition and crystallization kinetics of R_2O–Al_2O_3–SiO_2 glass–ceramics

Dehua Xiong*, Jinshu Cheng, Hong Li

Key Laboratory of Silicate Materials Science and Engineering, Wuhan University of Technology, Ministry of Education, Wuhan 430070, China

ARTICLE INFO

Article history:
Received 21 February 2010
Received in revised form 13 March 2010
Accepted 15 March 2010
Available online 23 March 2010

Keywords:
DSC
R_2O–Al_2O_3–SiO_2
Glass–ceramics
Crystallization kinetics

ABSTRACT

The crystallization behavior and microstructure of R_2O–Al_2O_3–SiO_2 (R means K, Na and Li) glass were investigated by means of differential scanning calorimeter (DSC), X-ray diffraction (XRD) and scanning electron microscopy (SEM). The crystallization kinetic parameters including the crystallization apparent activation energy (E_a), the Avrami parameter (n), glass transition temperature (T_g) and the activity energy of glass transition (E_t) were also measured with different methods. The results have shown that: the DSC traces of composition A parent glass have two different precipitation crystallization peaks corresponding to E_{a1}(A) = 151.4 kJ/mol (Li_2SiO_3) and E_{a2}(A) = 623.1 kJ/mol ($Li_2Si_2O_5$), the average value of n = 1.70 ($Li_2Si_2O_5$) for the surface crystallization and E_t(A) = 202.8 kJ/mol. And E_a(B) = 50.7 kJ/mol (Li_2SiO_3), the average value of n = 3.89 (Li_2SiO_3) for the bulk crystallization and E_t (B) = 220.4 kJ/mol for the composition B parent glass. Because of the content of R_2O is bigger than composition A, composition B parent glass has a lower E_a, T_g and a larger n, E_t.

1. Introduction

Currently there has been a considerable amount of interest on crystallization behavior and other thermo-physical properties Li_2O–ZnO–SiO_2 glass–ceramics due to their beneficial properties, e.g., a wide range of thermal expansion coefficients (from 50 to $200 \times 10^{-7}/^{\circ}C$) by controlling heat treatments, high electrical resistivity and good chemical durability. These properties coupled with wide range of TEC make this glass–ceramics material suitable for fabrication of hermetic seals to a variety of metals and alloys including copper, stainless steel, etc. A number of studies on crystallization behaviors and other thermo-physical properties in Li_2O–ZnO–SiO_2 glass–ceramics system have been carried out [1–5]. The properties of glass–ceramics are dependant on the chemical composition and the thermal history. It is therefore important to gain a thorough understanding of the processes in the crystallization of the glass–ceramics. Study on crystallization kinetics of glass–ceramics to explore the effects of compositions on crystallization properties of glass, optimized the composition and improved the performance of glass–ceramics have important theoretical significance.

Isothermal and non-isothermal analysis methods have been used for collecting kinetic dates with the minimum of experimental measurements during the studies of glass crystallization kinetics for many years. Though DTA and DSC were proven techniques, the calculation results obtained from different methods are controversial over the use of these methods to study the parameters of crystallization kinetics [4]. The present investigation has monitored the crystallization kinetics of R_2O–Al_2O_3–SiO_2 (RAS) glass by using a variety of isothermal and non-isothermal analysis techniques. The crystallization behavior and microstructure of RAS glasses containing P_2O_5 were investigated by means of DSC, XRD and SEM. The crystallization kinetic parameters including the crystallization apparent activation energy (E_a), the Avrami parameter (n) and the activity energy of glass transition (E_t) were also measured with different methods.

2. Theoretical considerations

In non-isothermal transformation studies, the peaks crystallization exothermic temperature (T_p) on DSC traces of glasses were affected by the heating rate β. The crystalline phases have sufficient time to grow and T_p was low, the instantaneous rate of transformation is small and the crystallization peak flat when the heating rate β was slow. On the contrary, the glass crystallization lag phase transition and T_p increased, the instantaneous rate of transformation is great and sharp peak exothermic crystallization with a faster heating rate. According to the above exothermic crystallization characteristics and JMA equation, we can use differential methods of thermal analysis to study the glass to facilitate crystallization kinetics and calculate kinetic parameters of crystallization of glass.

Kinetics data, including activation energies (E_a) for crystallization, has also been derived employing non-isothermal techniques. The Avrami parameter (n) could be calculated by using isothermal analysis techniques. For example, from knowledge of the variation in peak crystallization temperature with heating rate, as originally

* Corresponding author. Tel.: +86 027 87860801; fax: +86 027 87860801.
E-mail address: xiongdehua@whut.edu.cn (D. Xiong).

0925-8388/$ – see front matter © 2010 Elsevier B.V. All rights reserved.
doi:10.1016/j.jallcom.2010.03.143

Table 1
The main chemical composition of parent glass (wt%).

Composition	$SiO_2 + Al_2O_3 + ZnO$	Li_2O	K_2O	Na_2O	P_2O_5	Sb_2O_3	R_2O/SiO_2
A	71.82	7.68	8.10	6.96	2.24	0.00	0.35
B	71.82	6.57	10.55	9.05	2.01	0.5	0.40

described by Kissinger [6,7]. Kissinger proposed that the activation energy of a first order process can be determined from the variation in peak temperature with heating rate using DSC from the relationship [4]:

$$\ln \frac{\beta}{T_p^2} = -\frac{E_a}{RT_p} + C_1 \quad (1)$$

In Kissinger equation, β is the heating rate, T_p is the peak temperature (e.g. crystallization peak temperature), and E_a is the activation energy, often described as an apparent activation energy. Plot of $\ln(\beta/T_p^2)$ versus $1/T_p$ also is expected to be linear, and from the slop of the plot, the activation energy, E_a can be calculated.

The value of n can be attained from the following equation [8–10]:

$$\ln\ \Delta T = -\frac{nE_a}{RT_i} + C_3 \quad (2)$$

Here T_i is the random temperature in the DSC traces, ΔT is the vertical displacement from the baseline to the line of the crystallization exothermic peak at the temperature T_i. Plot of $\ln(\Delta T)$ versus $1/T_i$ also is expected to be linear, and from the slop of the plot is $-nE_a/R$, the Avrami parameter (n) can be calculated.

The relationship between the glass transition temperature T_g and the heating rate β can be discussed through the empirical equation:

$$T_g = A + B\ \ln \beta \quad (3)$$

where A and B are constants for a given glass composition [11,12]. Plot of T_g versus $\ln(\beta)$ for the prepared samples, the values of A and B can be obtained by using the least square fit, and this equation holds good for the studied samples. To obtain the activity energy of glass transition E_t, the data were fitted by the Kissinger method [7], which is most commonly used in analyzing crystallization data in DSC experiments. According to the Kissinger equation, the glass transition temperature T_g depends on the heating rate β as follows:

$$\ln \frac{\beta}{T_g^2} = -\frac{E_t}{RT_g} + C_4 \quad (4)$$

Based on the above relationship, plot of $\ln(\beta/T_g^2)$ versus $(1/T_g)$ for the prepared samples; slopes of these lines yield the values of E_t/R where E_t corresponds to the glass transition activation energy.

3. Experimental details

3.1. Preparation of parent glass

Based on our previous works [13–16], the composition of parent glass is shown in Table 1. All raw materials were chemical reagents with pure analysis; Sb_2O_3 was added as clarifier, P_2O_5 was used as compound nucleation agent. The reagents of SiO_2, Al_2O_3, Li_2CO_3, Na_2CO_3, K_2CO_3, ZnO, and $(NH_4)H_2PO_4$ were mixed and pulverized into powder in agate mortar, and then they were melted in the 200 ml alumina crucible at 1430–1460 °C for 3 h in an electric furnace. The melts were cast into the pre-heated graphite mold. Subsequently, the glass was annealed at 440–480 °C for 30 min and then cooled to room temperature in the furnace naturally. Finally, bulk transparent and parent glass without any bubbles were prepared.

3.2. Differential thermal analysis (DSC)

The parent glass were pulverized into powder (0.150–0.075 mm) suitable for DSC employing a NETZSCH (STA 449C) DSC with the temperature range of 20–1000 °C. The glass powder with the weight of 30 mg was contained in a platinum crucible and the reference material was α-Al_2O_3 powders. The data were recorded by means of a chart recorder. The samples were heated in air from ambient temperature to 1000 °C at heating rates of 5, 10, 15 and 20 °C/min.

3.3. X-ray diffraction (XRD)

The glass–ceramics were pulverized into powder in agate mortar and subjected to pass 200 meshes sieve for XRD analysis. The types of crystal phases after heat treatment were analyzed by XRD (Rigaku D/max-RA) using copper Kα radiation, produced at 35 kV and 30 mA, with 2θ = 10–60°and 0.02° per second, and the diffraction patterns were analyzed by the use of MDI Jade 5.0 software.

3.4. Scanning electron microscope (SEM)

For SEM (JSM-5610V) observation, the specimens which were polished by diamond slurry and chemically etched by 4 volume hydrofluoric acid for 30 s were used. The microstructures of crystal phases could be observed in this way.

4. Results and discussion

Typical DSC traces of two similar glass compositions crystallized at heating rates of 5, 10, 15 and 20 °C min^{-1} are shown in Figs. 1 and 2. The thermal parameters are summarized in Table 2, where T_g is the glass transition temperature (extrapolated onset), T_{p1} and T_{p2} are the first and second crystallization peak temperatures, respectively.

The endothermic base line shift at 425-460 °C (Fig. 1) indicates the glass transition temperature in case of composition A parent glass system and the sharp exothermic peaks at the onset values of 620–675 and 820–875 °C are two crystallization temperatures

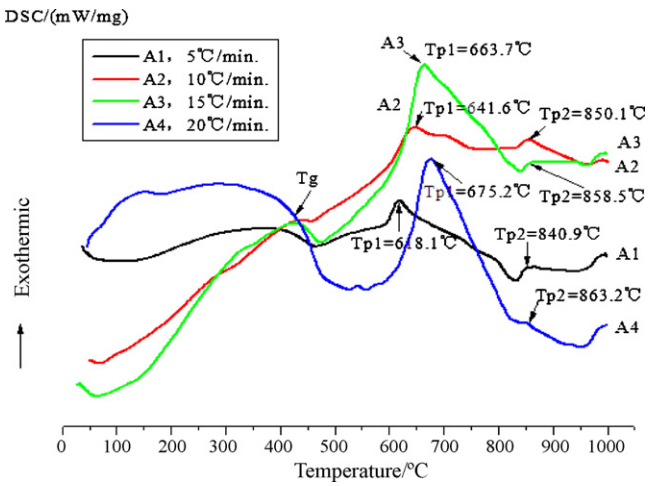

Fig. 1. DSC traces of the composition A glass.

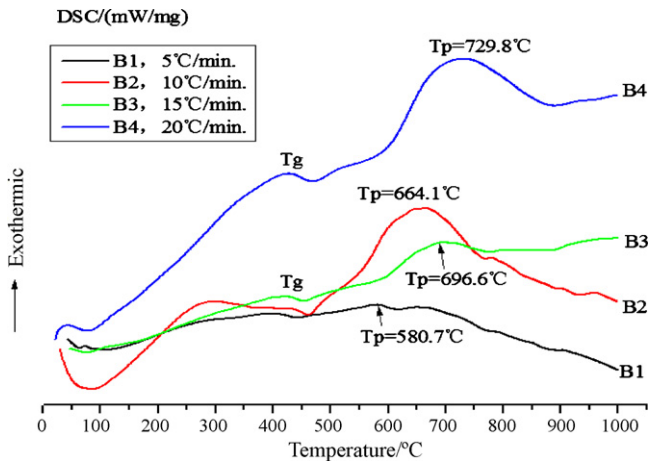

Fig. 2. DSC traces of the composition B glass.

Table 2
Thermal properties of parent glass.

Composition	β (°C/min)	T_g (°C)	T_{p1} (°C)	T_{p2} (°C)
A	5	432.9 ± 2	618.1 ± 2	840.9 ± 2
	10	444.2 ± 2	641.6 ± 2	850.1 ± 2
	15	454.0 ± 2	663.7 ± 2	858.5 ± 2
	20	460.4 ± 2	675.2 ± 2	863.2 ± 2
B	5	425.0 ± 2	580.7 ± 2	
	10	439.2 ± 2	664.1 ± 2	
	15	444.6 ± 2	696.6 ± 2	
	20	450.2 ± 2	729.8 ± 2	

for this system. For composition B, the glass transition temperature was observed at 445 °C and the crystallization peak at 730 °C while the heating rate was 20 °C min^{-1} (Fig. 2). It is seen that the glass transition temperature of composition B is lower compared to composition A, which is due to higher R_2O content in composition B sample.

Table 3
The heat treatment schedules of glass–ceramics.

Sample no.	Nucleate temperature (°C)	Nucleate time (h)	Crystal temperature (°C)	Crystal time (h)
A0	0	0	0	0
A1	500	3	650	3
A2	500	3	850	3
B0	0	0	0	0
B1	500	2	700	2
B2	500	2	750	2

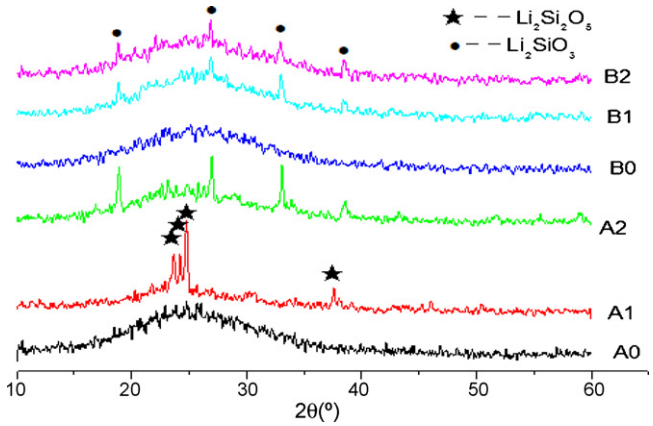

Fig. 3. The XRD patterns of samples.

4.1. Crystallization behaviors of glass–ceramics

Figs. 1 and 2 show the basis of DSC traces of glass, combined with previous works [13–16], the heat treatment schedules of glass–ceramics were shown in Table 3.

It was seen all samples have crystal phase except parent glasses (A0 and B0), and Li_2SiO_3 and $Li_2Si_2O_5$ were crystallized in glass–ceramics form in Fig. 3. Experimental results show that all the samples have the main crystal phase in the suitable heat treatment schedule, but the main crystal phase was changed with the

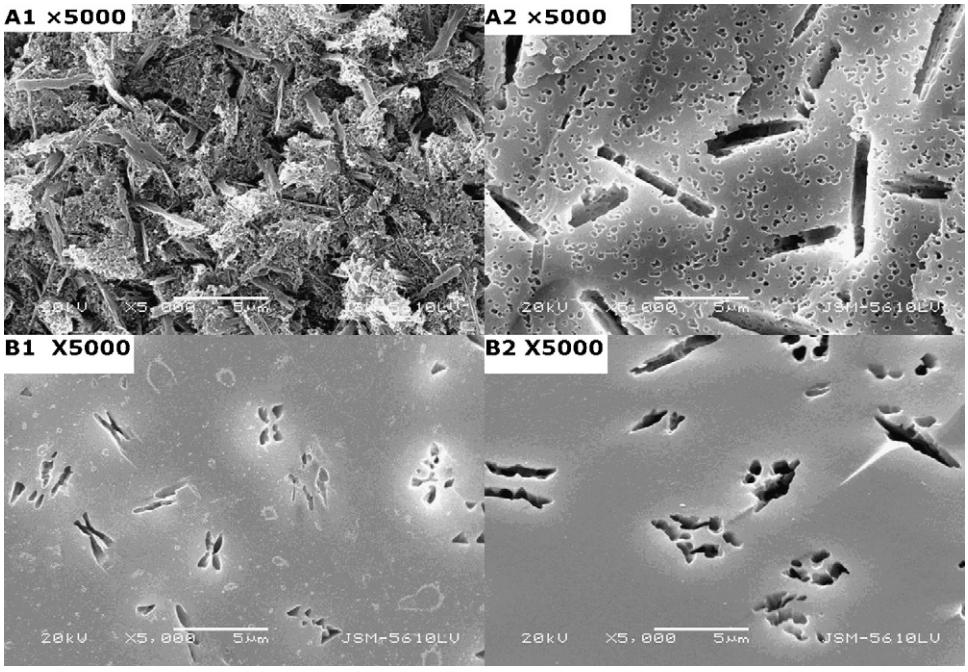

Fig. 4. SEM images of the crystal phases and microstructures of glass–ceramics.

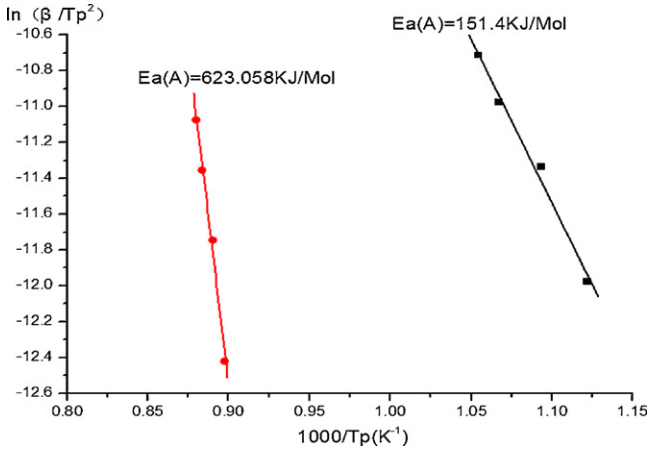

Fig. 5. Plots of $\ln(\beta/T_p^2) - 1/T_p$ for the composition A glass.

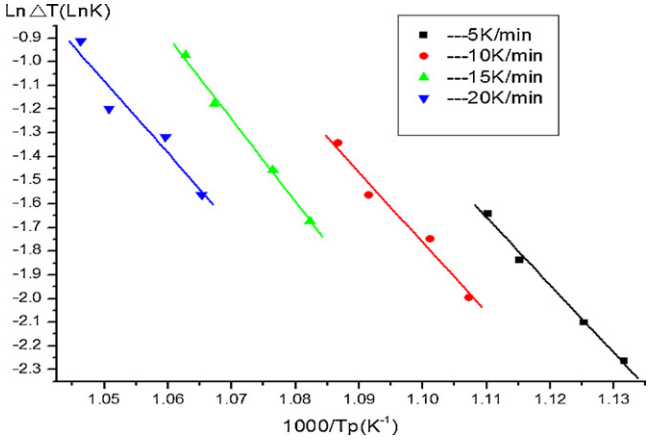

Fig. 7. Plots of $\ln(\Delta T) - 1/T_i$ for the composition A glass (LS_2).

heat treatment temperature and time changed. The main crystal phases of A2, B1 and B2 were Li_2SiO_3, but the main crystal phase of A1 was $Li_2Si_2O_5$. The main crystal phase changed from Li_2SiO_3 to $Li_2Si_2O_5$ as the crystal temperature increased which corresponds to the DSC traces have two exothermic peaks in composition A. As the parent glasses of the RAS system with P_2O_5 as nucleation agents, compared with composition A, so the crystallization capability of composition B was weak with the content of P_2O_5 in composition B has decreased.

The crystal phases and microstructures of glass–ceramics were investigated by SEM (see Fig. 4), the crystals of samples A2, B1 and B2 were needle-like Li_2SiO_3, A1 for the columnar $Li_2Si_2O_5$ which is consistent to the results of XRD, but the amount and size of crystallites are very small in all samples. Different from other glass–ceramics system, figure in black for the region to mean after the crystallites were etched, and the light for the regional shown the residual glass phase. Because all samples were chemically etched by hydrofluoric acid, the etched rate of Li_2SiO_3 is much greater than glass phase. Experimental results show that all the samples have main crystal phases under the suitable heat treatment schedule, but the amount and size of crystallites in sample changed with the heat treatment temperature changed. The crystallites grew and the glass phase decreased as the crystal temperature and crystal time increased, and the shape of crystallites even more obvious.

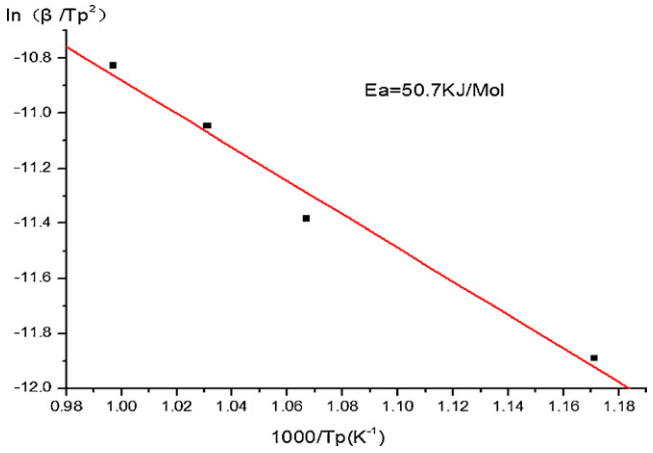

Fig. 6. Plots of $\ln(\beta/T_p^2) - 1/T_p$ for the composition B glass.

4.2. Activation energy (E_a) of parent glass

Values calculated for the activation energies (E_a) using the Kissinger method (Eq. (1)). Plot of $\ln(\beta/T_p^2)$ versus $1/T_p$ also is expected to be linear, and from the slop of the plot, the activation energy, E_a can be calculated. Experimental non-isothermal plots are summarized in Figs. 5 and 6.

The activation energy for the composition A parent glass which have two exothermic peaks on the DSC traces, the first crystalline phase to form (peak 1) is determined as 151.4 kJ/mol and the second crystalline phase to form (peak 2) is determined as 623.1 kJ/mol by the Kissinger method. The activation energy for the composition B glass, the crystalline phase to form is determined as 50.7 kJ/mol by the Kissinger method. Derived as a result of the method of calculation errors, it could get a qualitative change in the trend of the results, in order to have an accurate calculation of the results also need to continually improve.

4.3. Avrami parameter (n) of parent glass

For the determination of the crystallization mechanism, the crystallization kinetics parameters n and m depending on the nucleation process and growth morphology, the value of m can be deduced from $n = m + 1$ [17,18]. $m = 1$ shows that for the crystallization of glass surface crystallization; $m = 2$ shows that the glass crystallization for two-dimensional crystallization; $m \geq 3$ shows that the crystallization of glass for the bulk or three-dimensional crystallization. Since the DSC trace of composition A parent glass has two different precipitation crystallization peaks corresponding to different crystals, so we choose the first crystallization peak to calculate the value n of the crystal LS_2. The Avrami parameter (n) of parent glass can be calculated from Eq. (2), plot of $\ln(\Delta T)$ versus $1/T_i$ also is expected to be linear, and from the slop of the plot is $-nE_a/R$, the Avrami parameter (n) can be calculated, experimental isothermal plots are summarized in Figs. 7 and 8 and Table 4.

The results show that: the average value of $n = 1.70$, $m = 0.7$ with L_2S crystal in composition A for the surface crystallization; in composition B, the average value of $n = 3.89$, $m = 2.89$ with LS crystal for the bulk crystallization. As the two group parent glass, the Li_2O has participated in the formation of the main crystal phase, as well as the variety of the main crystal phase in two groups lead to the growth of main crystalline phase exists differences in crystallization.

Table 4
The Avrami parameter (n) of parent glass.

Crystal	Avrami parameter (n)				
	$\beta = 5\,^{\circ}C\,min^{-1}$	$\beta = 10\,^{\circ}C\,min^{-1}$	$\beta = 15\,^{\circ}C\,min^{-1}$	$\beta = 20\,^{\circ}C\,min^{-1}$	Average value
LS_2(A)	1.57	1.63	1.91	1.67	1.70
LS(B)	4.53	3.95	3.80	3.29	3.89

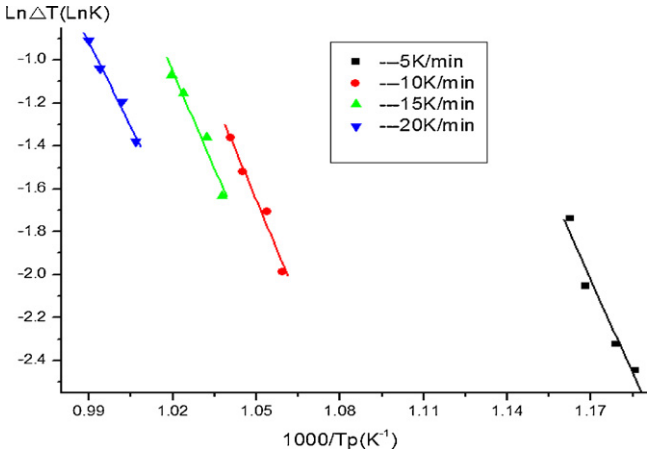

Fig. 8. Plots of $\ln(\Delta T) - 1/T_i$ for the composition B glass (LS).

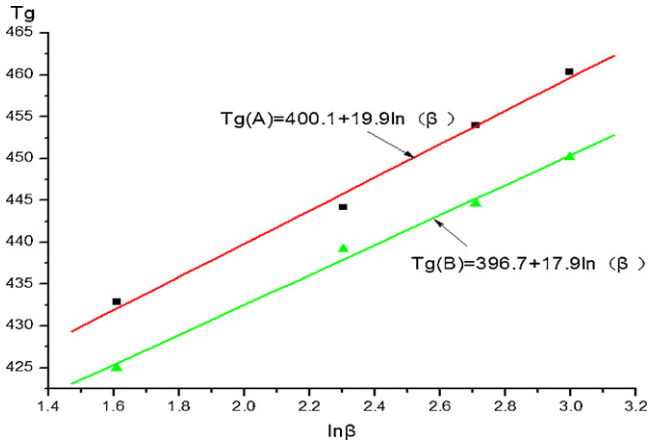

Fig. 9. Plots of $T_g - \ln(\beta)$ for the parent glass.

4.4. Transition activation energy (E_t) of parent glass

In order to design the new glasses well and perform nano-crystallization on the glasses properly, it is necessary to understand the influence of alkali metal oxides addition on the thermal properties and crystallization kinetics of the glasses. From Eqs. (3) and (4), plots of T_g versus $\ln(\beta)$ for the prepared samples, the values of A and B (A and B are constants for a given glass composition) can be obtained by using the least square fit, and this equation holds good for the studied samples (as shown in Fig. 9). To obtain the activity energy of glass transition E_t, straight lines between $\ln(\beta/T_g^2)$ and $(1000/T_g)$ can be given; slopes of these lines yield the values of E_t/R where E_t corresponds to the glass transition activation energy (as shown in Fig. 10). From Figs. 9 and 10, we can see that the two composition glass have got a similar results, there was a little difference between the two glasses. For composition A, $T_g(A) = 400.1 + 19.9 \ln \beta$, $E_t(A) = 202.8$ kJ/mol; and composition B, $T_g(B) = 396.7 + 17.9 \ln \beta$, $E_t(B) = 220.4$ kJ/mol; as shown in Table 5.

From Table 5, composition A parent glass has a higher glass transition temperature, the smaller the transition activation energy.

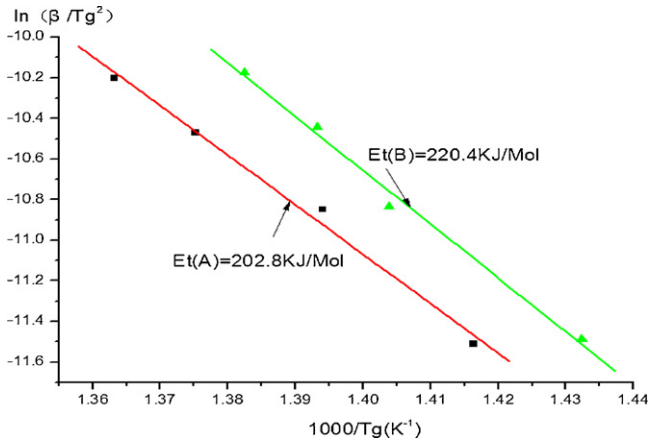

Fig. 10. Plots of $\ln(\beta/T_g^2) - 1/T_g$ for the parent glass.

Table 5
The value A, B and E_t of parent glass.

Composition	A (K)	B (K)	E_t (kJ/mol)
A	400.1	19.9	202.8
B	396.7	17.9	220.4

Because the content of R_2O is bigger than composition A, composition B parent glass has a lower glass transition temperature and larger glass transition activation energy.

5. Conclusions

(1) After heat treatment, the main crystal phase columnar $Li_2Si_2O_5$ were found when crystallization temperature is 650 °C and the needle-like Li_2SiO_3 crystals while crystallization temperature is 850 °C in composition A parent glass; the main crystal phase needle-like Li_2SiO_3 were found when crystallization temperature is 700 °C and 750 °C in the composition B parent glass.
(2) Values calculated for the activation energies (E_a) using the Kissinger method, the first crystalline phase to form (peak 1) is determined as $E_{a1}(A) = 151.4$ kJ/mol and the second crystalline phase to form (peak 2) is determined as $E_{a2}(A) = 623.1$ kJ/mol in composition A parent glass; the crystalline phase to form is determined as $E_a(B) = 50.7$ kJ/mol for the composition B parent glass.
(3) The average value of $n = 1.70$, $m = 0.7$ with L_2S crystal in composition A for the surface crystallization; in composition B, the average value of $n = 3.89$, $m = 2.89$ with LS crystal for the bulk crystallization.
(4) Compared to composition A, composition B parent glass has a lower glass transition temperature and larger glass transition activation energy, $E_t(A) = 202.8$ kJ/mol and $E_t(B) = 220.4$ kJ/mol, respectively.

Acknowledgements

The authors would like to express sincere thanks for the financial supports by National Natural Science Foundation

of China (50472039) and Hubei Natural Science Foundation (2005ABA011).

References

[1] B.I. Sharma, M. Goswami, et al., Mater. Lett. 58 (2004) 2423–2438.
[2] S. Cramer von Clausbruch, et al., J. Non-Cryst. Solids 263–264 (2000) 388–394.
[3] Z.X. Chen, P.W. McMillan, J. Am. Ceram. Soc. 4 (1985) 220–224.
[4] I.W. Donald, J. Non-Cryst. Solids 345–346 (2004) 120–126.
[5] M. Goswami, P. Sengupta, et al., Ceram. Int. 33 (2007) 863–867.
[6] H.E. Kissinger, Anal. Chem. 11 (1957) 1702–1706.
[7] H.E. Kissinger, J. Res. Nat. Bur. Stand. 57 (1956) 217.
[8] H. Shao, K. Liang, F. Peng, Ceram. Int. 30 (2004) 927–930.
[9] M. Avrami, J. Chem. Phys. 7 (1939) 1103.
[10] G.O. Piloyan, I.D. Ryabchikov, O.S. Novikova, Nature (London) 212 (1966) 1229.
[11] M. Lasocka, Mater. Sci. Eng. 23 (1976) 173–177.
[12] C. Liu, G. Tang, L. Luo, W. Chen, J. Alloys Compd. 474 (2009) 468–472.
[13] H. Li, J. Cheng, X. Cao, T. Wang, Key Eng. Mater. 336–338 (2007) 1862–1864.
[14] H. Li, Y. Du, J. Cheng, T. Wang, Key Eng. Mater. 368–372 (2008) 1436–1438.
[15] D. Xiong, J. Cheng, H. Li, W. Deng, K. Ye, Microelectron. Eng. (2009), doi:10.1016/j.mee.2009.10.001.
[16] D. Xiong, J. Cheng, J. Wuhan Univ. Technol. 22 (2009) 40–43, in Chinese.
[17] Y. Cheng, H. Xiao, W. Guo, W. Guo, Thermochim. Acta 444 (2006) 173–178.
[18] R. Iordanova, E. Lefterova, I. Uzunov, D. Klissurshi, J. Therm. Anal. Calorim. 70 (2002) 393–404.